

Spectral phase conjugation via temporal imaging

Onur Kuzucu,^{1,*} Yoshitomo Okawachi,¹ Reza Salem,¹ Mark A. Foster,¹
Amy C. Turner-Foster,² Michal Lipson,² and Alexander L. Gaeta¹

¹*School of Applied and Engineering Physics, Cornell University, Ithaca, NY 14853*

²*School of Electrical and Computer Engineering, Cornell University, Ithaca, NY 14853*

*ook2@cornell.edu

Abstract: We experimentally demonstrate wavelength-preserving spectral phase conjugation for compensating chromatic dispersion and self-phase modulation in optical fibers. Our implementation is based on a temporal imaging scheme that uses time lenses realized by broadband four-wave mixing in silicon waveguides. By constructing a temporal analog of a 4-*f* imaging system, we compensate for pulse distortions arising from second- and third-order dispersion and self-phase modulation in optical fibers.

©2009 Optical Society of America

OCIS codes: (190.4390) Nonlinear optics, integrated optics; (190.4380) Nonlinear optics, four-wave mixing; (230.2035) Dispersion compensation devices.

References and Links

1. S. Watanabe, and M. Shirasaki, "Exact compensation for both chromatic dispersion and Kerr effect in a transmission fiber using optical phase conjugation," *IEEE J. Lightwave Tech.* **14**(3), 243–248 (1996).
2. A. Yariv, D. Fekete, and D. M. Pepper, "Compensation for channel dispersion by nonlinear optical phase conjugation," *Opt. Lett.* **4**(2), 52–54 (1979).
3. D. A. B. Miller, "Time reversal of optical pulses by four-wave mixing," *Opt. Lett.* **5**(7), 300–302 (1980).
4. M. Tsang, and D. Psaltis, "Dispersion and nonlinearity compensation by spectral phase conjugation," *Opt. Lett.* **28**(17), 1558–1560 (2003).
5. M. C. Tatham, G. Sherlock, and L. D. Westbrook, "Compensation fibre chromatic dispersion by optical phase conjugation in a semiconductor laser amplifier," *Electron. Lett.* **29**(21), 1851–1852 (1993).
6. D. F. Geraghty, R. B. Lee, M. Verdiell, M. Ziari, A. Mathur, and K. J. Vahala, "Wavelength conversion for WDM communication systems using four-wave mixing in semiconductor optical amplifiers," *IEEE J. Sel. Top. Quantum Electron.* **3**(5), 1146–1155 (1997).
7. J. Inoue, H. Sotobayashi, W. Chujo, and H. Kawaguchi, "80 Gbit/s OTDM signal transmission over 208 km standard fibre using midspan optical phase conjugation based on four-wave mixing in semiconductor optical amplifiers," *Electron. Lett.* **38**(15), 819–821 (2002).
8. S. Watanabe, T. Naito, and T. Chikama, "Compensation of chromatic dispersion in a single-mode fiber by optical phase conjugation," *IEEE Photon. Technol. Lett.* **5**(1), 92–95 (1993).
9. A. H. Gnauck, R. M. Jopson, and R. M. Derosier, "10-Gb/s 360-km transmission over dispersive fiber using midsystem spectral inversion," *IEEE Photon. Technol. Lett.* **5**(6), 663–666 (1993).
10. S. Watanabe, T. Chikama, G. Ishikawa, T. Terahara, and H. Kuwahara, "Compensation of pulse shape distortion due to chromatic dispersion and Kerr effect by optical phase conjugation," *IEEE Photon. Technol. Lett.* **5**(10), 1241–1243 (1993).
11. P. Minzioni, I. Cristiani, V. Degiorgio, L. Marazzi, M. Martinelli, C. Langrock, and M. M. Fejer, "Experimental demonstration of nonlinearity and dispersion compensation in an embedded link by optical phase conjugation," *IEEE Photon. Technol. Lett.* **18**(9), 995–997 (2006).
12. S. Watanabe, G. Ishikawa, T. Naito, and T. Chikama, "Generation of optical phase-conjugate waves and compensation for pulse shape distortion in a single-mode fiber," *IEEE J. Lightwave Tech.* **12**(12), 2139–2146 (1994).
13. S. Ayotte, H. Rong, S. Xu, O. Cohen, and M. J. Paniccia, "Multichannel dispersion compensation using a silicon waveguide-based optical phase conjugator," *Opt. Lett.* **32**(16), 2393–2395 (2007).
14. S. Ayotte, S. Xu, H. Rong, and M. J. Paniccia, "Dispersion compensation by optical phase conjugation in silicon waveguide," *Electron. Lett.* **43**(19), 1037–1039 (2007).
15. K. Inoue, "Spectral inversion with no wavelength shift based on four-wave mixing with orthogonal pump beams," *Opt. Lett.* **22**(23), 1772–1774 (1997).
16. A. M. Weiner, D. E. Leaird, D. H. Reitze, and E. G. Paek, "Femtosecond spectral holography," *IEEE J. Quantum Electron.* **28**(10), 2251–2261 (1992).
17. A. M. Weiner, D. E. Leaird, D. H. Reitze, and E. G. Paek, "Spectral holography of shaped femtosecond pulses," *Opt. Lett.* **17**(3), 224–226 (1992).
18. C. Joubert, M. L. Roblin, and R. Grousson, "Temporal reversal of picosecond optical pulses by holographic phase conjugation," *Appl. Opt.* **28**(21), 4604–4612 (1989).

19. M. L. Roblin, F. Gires, R. Grousson, and P. Lavallard, "Enregistrement par holographie de volume d'une loi de phase spectrale: Application a la compression d'impulsion picoseconde," *Opt. Commun.* **62**(3), 209–214 (1987).
20. D. M. Marom, D. Panasenکو, R. Rokitski, P.-C. Sun, and Y. Fainman, "Time reversal of ultrafast waveforms by wave mixing of spectrally decomposed waves," *Opt. Lett.* **25**(2), 132–134 (2000).
21. D. M. Marom, D. Panasenکو, P.-C. Sun, Y. T. Mazurenko, and Y. Fainman, "Real-time spatial-temporal signal processing with optical nonlinearities," *IEEE J. Sel. Top. Quantum Electron.* **7**(4), 683–693 (2001).
22. H. Nishioka, S. Ichihashi, and K. Ueda, "Frequency-domain phase-conjugate femtosecond pulse generation using frequency resolved crossphase modulation," *Opt. Express* **10**(18), 920–926 (2002).
23. T. T. Ng, F. Parmigiani, M. Ibsen, Z. ZhaoWei, P. Petropoulos, and D. J. Richardson, "Compensation of linear distortions by using XPM with parabolic pulses as a time lens," *IEEE Photon. Technol. Lett.* **20**(13), 1097–1099 (2008).
24. H. Nishioka, H. Tomita, K. Hayasaka, and K. Ueda, "All-optical temporal phase correction scheme for few-cycle optical pulses using diffractive optics," *Opt. Express* **14**(16), 7447–7455 (2006).
25. V. L. da Silva, Y. Silberberg, J. P. Heritage, E. W. Chase, M. A. Saifi, and M. J. Andrejco, "Femtosecond accumulated photon echo in Er-doped fibers," *Opt. Lett.* **16**(17), 1340–1342 (1991).
26. N. W. Carlson, L. J. Rothberg, A. G. Yodh, W. R. Babbitt, and T. W. Mossberg, "Storage and time reversal of light pulses using photon echoes," *Opt. Lett.* **8**(9), 483–485 (1983).
27. B. H. Kolner, "Space-time duality and the theory of temporal imaging," *IEEE J. Quantum Electron.* **30**(8), 1951–1963 (1994).
28. C. V. Bennett, and B. H. Kolner, "Principles of parametric temporal imaging - Part I: System configurations," *IEEE J. Quantum Electron.* **36**(4), 430–437 (2000).
29. C. V. Bennett, and B. H. Kolner, "Principles of parametric temporal imaging - Part II: System performance," *IEEE J. Quantum Electron.* **36**(6), 649–655 (2000).
30. S. Kumar, "Compensation of third-order dispersion using time reversal in optical transmission systems," *Opt. Lett.* **32**(4), 346–348 (2007).
31. D. F. Geraghty, R. Salem, M. A. Foster, and A. L. Gaeta, "A simplified optical correlator and its application to packet-header recognition," *IEEE Photon. Technol. Lett.* **20**(7), 487–489 (2008).
32. J. W. Goodman, *Introduction to Fourier Optics*, (McGraw-Hill, San Francisco, CA, 1968).
33. F. Li, and J. Azaña, "Simplified system configuration for real-time Fourier transformation of optical pulses in amplitude and phase," *Opt. Commun.* **274**(1), 59–65 (2007).
34. J. Azaña, N. K. Berger, B. Levit, and B. Fischer, "Spectral Fraunhofer regime: time-to-frequency conversion by the action of a single time lens on an optical pulse," *Appl. Opt.* **43**(2), 483–490 (2004).
35. M. T. Kauffman, W. C. Banyai, A. A. Godil, and D. M. Bloom, "Time-to-frequency converter for measuring picosecond optical pulses," *Appl. Phys. Lett.* **64**(3), 270–272 (1994).
36. M. A. Foster, R. Salem, D. F. Geraghty, A. C. Turner-Foster, M. Lipson, and A. L. Gaeta, "Silicon-chip-based ultrafast optical oscilloscope," *Nature* **456**(7218), 81–84 (2008).
37. M. A. Foster, A. C. Turner, J. E. Sharping, B. S. Schmidt, M. Lipson, and A. L. Gaeta, "Broad-band optical parametric gain on a silicon photonic chip," *Nature* **441**(7096), 960–963 (2006).
38. R. Salem, M. A. Foster, A. C. Turner, D. F. Geraghty, M. Lipson, and A. L. Gaeta, "Optical time lens based on four-wave mixing on a silicon chip," *Opt. Lett.* **33**(10), 1047–1049 (2008).
39. R. Salem, M. A. Foster, A. C. Turner-Foster, D. F. Geraghty, M. Lipson, and A. L. Gaeta, "High-speed optical sampling using a silicon-chip temporal magnifier," *Opt. Express* **17**(6), 4324–4329 (2009).
40. Y. Okawachi, R. Salem, M. A. Foster, A. C. Turner-Foster, M. Lipson, and A. L. Gaeta, "High-resolution spectroscopy using a frequency magnifier," *Opt. Express* **17**(7), 5691–5697 (2009).
41. M. A. Foster, R. Salem, Y. Okawachi, A. C. Turner-Foster, M. Lipson, and A. L. Gaeta, "Ultrafast waveform compression using a time-domain telescope," *Nat. Photonics* **3**(10), 581–585 (2009).
42. D. Méchin, R. Provo, J. D. Harvey, and C. J. McKinstrie, "180-nm wavelength conversion based on Bragg scattering in an optical fiber," *Opt. Express* **14**(20), 8995–8999 (2006).
43. C. McKinstrie, J. Harvey, S. Radic, and M. Raymer, "Translation of quantum states by four-wave mixing in fibers," *Opt. Express* **13**(22), 9131–9142 (2005).
44. M. J. Potasek, G. P. Agrawal, and S. C. Pinault, "Analytic and numerical study of pulse broadening in nonlinear dispersive optical fibers," *J. Opt. Soc. Am. B* **3**(2), 205–211 (1986).
45. A. H. Gnauck, and R. M. Jopson, in *Optical Fiber Telecommunications IIIA*, I. P. Kaminov and T. L. Koch eds. (Academic Press, San Diego, 1997), p. 186.
46. I. Brener, B. Mikkelsen, K. Rottwitz, W. Burkett, G. Raybon, J. B. Stark, K. Parameswaran, M. H. Chou, M. M. Fejer, E. E. Chaban, R. Harel, D. L. Philen, and S. Kosinski, "Cancellation of all Kerr nonlinearities in long fiber spans using a LiNbO₃ phase conjugator and Raman amplification," in *Optical Fiber Communication Conference 2000*, **4**, 266–268 (2000).

1. Introduction

Practical limitations to high-speed communications in long-haul optical fibers arise from various linear and nonlinear distortions due to propagation through the medium. Specifically, linear loss, chromatic dispersion, and nonlinear interactions due to the $\chi^{(3)}$ nonlinearity in optical fibers cause waveform degradation which results in higher bit error rates at the receiver end. Recovering the information content by utilizing various signal recovery and

compensation techniques is a well-studied topic. While passive dispersion management methods exist such as the use of dispersion-shifted or dispersion-compensating fiber, active compensation methods come with the added benefit of compensating for dynamic distortions including removal of additional degradations incurred in pulse propagation. For example mid-point temporal phase conjugation (TPC) [1,2] and spectral phase conjugation (SPC) [3,4] have been shown to be effective in compensating for the effects of group-velocity dispersion (GVD) and Kerr nonlinearity in optical fibers. Although experimental demonstrations of TPC [5–15] are more prevalent than SPC, comparison of the two schemes shows that SPC can provide more extensive dispersion compensation performance [4]. Specifically, SPC offers the potential to compensate for *all* orders of dispersion and some of the nonlinear effects in optical fibers such as self-phase modulation (SPM) and self steepening (SS), whereas TPC can compensate only for even-orders of dispersion, SPM, and intra-pulse Raman scattering (IRS) [4]. Among these nonlinear effects, SPM typically induces the shortest effective length for practical pulse and fiber parameters [4], which makes SPM compensation more critical than SS or IRS compensation. To date, dispersion compensation by SPC has been demonstrated with spectral and temporal holography [16–19], three-wave mixing in $\chi^{(2)}$ nonlinear media [20,21], cross-phase modulation [22,23], two-photon absorption [24], and photon echo measurements in inhomogeneously broadened media [25,26]. While most of these SPC implementations have focused on GVD compensation, the potential for compensating the higher-order dispersive and nonlinear effects has not been sufficiently exploited. Furthermore, SPC configurations that utilize three- or four-wave mixing (FWM) carry an additional drawback due to the introduction of a frequency shift to the input signal, which may be undesirable in practice.

We introduce temporal imaging as an alternative method to address these issues and perform SPC with its dispersion and nonlinear compensation capabilities for optical communications. Temporal imaging has proven to be an extremely flexible technique to perform several all-optical information processing tasks efficiently [27–29]. Much like beam shaping in Fourier optics, temporal imaging provides the capability to engineer the amplitude and phase profile of a given electric field in the time domain. This scheme utilizes a time lens, which functions as a temporal analog of a spatial lens, enabling time-domain manipulation of a given input waveform [27].

In this article, we explore the capabilities of temporal imaging as a practical alternative to perform dispersion and nonlinearity compensation in optical fibers. Namely, we use a temporal imaging scheme that functions as a time-domain analog of a 4-*f* imaging system [30,31] with the extended capability to reverse and conjugate the distorted electric fields to realize SPC operation. Broadband and efficient FWM afforded by silicon waveguides is utilized to implement time lenses in our setup. We characterize the SPC performance for GVD, third-order dispersion (TOD) and SPM introduced by various optical fibers and verify excellent compensation for these effects in a wavelength preserving manner. We also discuss the performance limitations of our system and suggest improvements for future implementations.

2. Temporal imaging system

Fourier analysis is one of the most fundamental applications of a single-lens imaging system [32]. Implementing a Fourier analyzer in the spatial domain is straightforward. By exploiting space-time duality whereby paraxial beam propagation of spatial domain is replaced by dispersive pulse broadening [33,34] and a time lens is introduced by imparting quadratic phase modulation in the time domain [27], a complete time-domain analog of a Fourier analyzer can be constructed. This design requires two equal, dispersive propagation segments separated by a time lens of a focal length that matches the group-delay dispersion (GDD) in each segment [34–36]. While the quadratic phase modulation required for the time lens can be realized by an optical phase modulator, the numerical aperture and resolution capabilities of the lens can be greatly enhanced by imparting the phase modulation through wave-mixing

with chirped pulses in $\chi^{(2)}$ and $\chi^{(3)}$ nonlinear media [28]. We note that efficient and broadband FWM in silicon waveguides [36,37] has proven to be a highly effective technique to implement time lenses with excellent resolution and record length performance. Furthermore, FWM-based temporal imaging permits the use of sources at telecommunication wavelengths with close spectral proximity, unlike configurations based on sum- or difference-frequency generation. Recently, FWM-based Fourier analyzers and more advanced temporal imaging systems with multiple time lenses have been demonstrated to perform all-optical ultrafast waveform characterization tasks such as time-to-frequency conversion [35,36], temporal [38,39] and spectral [40] waveform magnification, and packet compression [41].

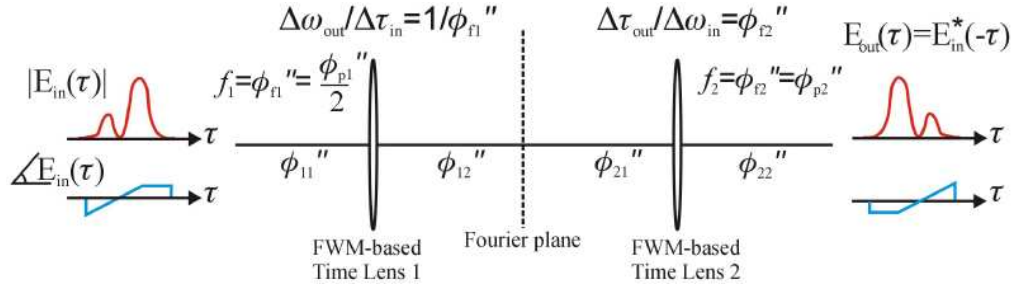


Fig. 1. (Color online) Spatial analog of the temporal imaging system for spectral phase conjugation. Input electric field envelope (red) and phase (blue) are transformed by a two-stage FWM configuration to generate an output field with temporal reversal and phase conjugation, i.e. $E_{out}(\tau) \propto E_{in}^*(-\tau)$. The amplitude (red) and phase (blue) of sample input and output electric fields are sketched for ideal SPC operation.

While most of these temporal imaging schemes characterize or manipulate the input field amplitude, one can also control the temporal or spectral phase profile of the input, which can be used for active dispersion compensation schemes [30]. We note that a temporal analog of a $4-f$ imaging system can be utilized for conjugating the spectral phase of a given input waveform after a set of modifications. From the properties of the Fourier transformation we observe that the conjugation operation in the frequency domain corresponds to conjugation *and* reversal in the time domain. Hence the temporal $4-f$ system using two time lenses should be able to revert and conjugate any given input waveform as sketched in Fig. 1. This requires that the overall waveform magnification factor should be set to -1 , and only one of the FWM operations generates an idler output proportional to the conjugate of the signal input in time domain. In this arrangement, the first lens acts as a Fourier analyzer to convert temporal information to the frequency domain with a time-to-frequency conversion factor of $\Delta\omega_{out}/\Delta\tau_{in} = -1/\phi_{f1}''$, where ϕ_{f1}'' corresponds to the focal length of the first time lens determined by the FWM pump GDD, $\phi_{f1}'' = -\phi_{p1}''/2 = -\beta_{p1}^{(2)}L_{p1}/2$, where $\beta_{p1}^{(2)}$ and L_{p1} are the GVD and length of the fiber through which the unchirped pump passes. The idler output after the first time lens can be related to the Fourier transform of the input signal electric field, $E_{in}(\omega) = \mathcal{F}\{E_{in}(\tau)\}$ as,

$$E_{idler,1}(\tau) = \mathcal{F}^{-1}\left\{\left[E_{in}^*(-\omega)G_{11}^*(-\omega)\right] \otimes H_1(\omega)\right\} G_{12}(\omega), \quad (1)$$

where $\mathbf{G}_{11}(\omega)$ and $\mathbf{G}_{12}(\omega)$ are the dispersion operators before and after the first time lens, respectively, $G_{jk}(\omega) = \exp(-i\phi_{jk}''\omega^2/2)$, and $\phi_{jk}'' = \beta_{jk}^{(2)}L_{jk}$. The time-lens operator, $\mathbf{H}_1(\omega) = \exp(i\phi_{f1}''\omega^2/2)$ represents the quadratic phase modulation introduced by FWM with the chirped pump pulse. Since the first FWM interaction uses a single pump input, the generated idler field is proportional to the conjugate of the signal field, i.e.

$E_{idler,1}(\tau) \propto E_{p1}^2(\tau)E_{in}^*(\tau)$. The quadratic phase modulation in the convolution integral of Eq. (1) can be cancelled when the pump dispersion $\phi_{p1}'' = \beta_{p1}^{(2)}L_{p1}$ is twice the input dispersion $\phi_{i1}'' = \beta_{i1}^{(2)}L_{i1}$ [38]. This situation is analogous to the spatial case where an object is placed a focal length away from a lens and the phase modulation on the transverse beam profile is cancelled by the lens. Furthermore, the residual chirp on the generated idler is compensated when the time-lens output dispersion has the negative sign of the input dispersion, i.e. $\phi_{i2}'' = -\phi_{i1}''$. The sign change in dispersion is required due to the conjugation of the signal field in the first FWM operation which utilizes a single pump input as sketched in the wavelength layout of Fig. 2(a). When these conditions are satisfied, the idler spectral content at the Fourier plane is proportional to the time-domain profile of the input waveform, realizing time-to-frequency conversion.

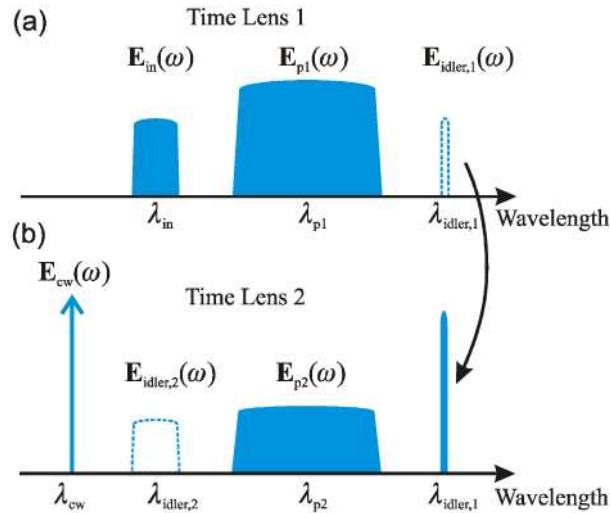


Fig. 2. (Color online) Wavelength layout of the two FWM processes to implement time reversal and conjugation of the input waveforms for realizing wavelength-preserving SPC operation. The idler output of the first FWM operation is amplified and used as one of the pump inputs to the second FWM stage to provide single conjugation for the signal field. The center wavelength of the quasi-cw source is adjusted to generate the second idler output at the original signal wavelength. The input fields to each stage are sketched with solid fill whereas the generated outputs are drawn with dashed lines.

The idler output of the first FWM process is directed to the second time lens which performs frequency-to-time conversion. Similar to the first time lens, the focal length ϕ_{f2}'' determines the scaling between the frequency-domain input and time-domain output, i.e. $\Delta\tau_{out} / \Delta\omega_{in} = -\phi_{f2}''$. In order to perform the SPC operation, the input electric field should be conjugated only once within the temporal imaging system. Note that the first FWM operation using a single pump already generates an idler output proportional to the conjugated signal input. Hence it is necessary to avoid consecutive conjugation in the second FWM stage. For this purpose we utilize a nondegenerate pump FWM configuration reminiscent of Bragg scattering in optical fibers [42,43] in which the output from the first FWM stage is used as one of the two pumps with the second pump being a quasi-cw source. In this configuration the center wavelength of the quasi-cw source can be adjusted to generate the idler output of the second FWM operation at the center wavelength of the system input, yielding a wavelength preserving operation as shown in Fig. 2(b). The quadratic phase modulation for the second time-lens operator is provided with a chirped probe input, which is conjugated in the second FWM process such that $E_{idler,2}(\tau) \propto E_{idler,1}(\tau)E_{p2}^*(\tau)$, where the quasi-cw field with longer

duration is taken as a constant. In our case, the probe is obtained from the unchirped pump input of the first FWM stage. Thus, the focal length of the second time lens is determined by the probe GDD, $\phi_{f2}'' = -\phi_{p2}''$. The imaging system output can be also expressed in terms of the dispersion operators and the second time-lens operator as,

$$E_{idler,2}(\tau) = \mathcal{F}^{-1} \left\{ \left[(\mathbf{E}_{idler,1}(\omega) \mathbf{G}_{21}(\omega)) \otimes \mathbf{H}_2^*(-\omega) \right] \mathbf{G}_{22}(\omega) \right\}. \quad (2)$$

Frequency-to-time conversion in the second lens requires the cancellation of the quadratic phase modulation in the convolution integral of Eq. (2). This condition is satisfied by adjusting the dispersion of the second time-lens input, output and probe paths such that $\phi_{21}'' = \phi_{22}'' = \phi_{p2}''$. Thus using Eqs. (1) and (2), it can be shown that the system output is related to the input field, $E_{out}(\tau) = E_{idler,2}(\tau) \propto E_{in}^*(\tau/\eta)$. The overall temporal scaling factor η between the system input and output fields is determined by the ratio $\eta = \phi_{f2}'' / \phi_{f1}''$, which can be set to -1 to realize SPC operation. Once the above requirements for the two cascaded Fourier analyzers and the temporal scaling factor are satisfied, one can entirely determine the lengths of dispersive fibers of the temporal imaging system relative to one free parameter. In our case, we determine the fiber lengths with respect to the input fiber GDD ϕ_{11}'' of the first FWM process. Hence, SPC operation is realized provided that $\phi_{12}'' = \phi_{21}'' = \phi_{22}'' = -\phi_{11}''$ and $\phi_{p1}'' / 2 = -\phi_{p2}'' = \phi_{11}''$. We further note that choosing different focal lengths for two time lenses enables temporal and spectral scaling of waveforms ($\eta \neq -1$) as demonstrated by recent time-lens-based all-optical signal processing experiments [38–41].

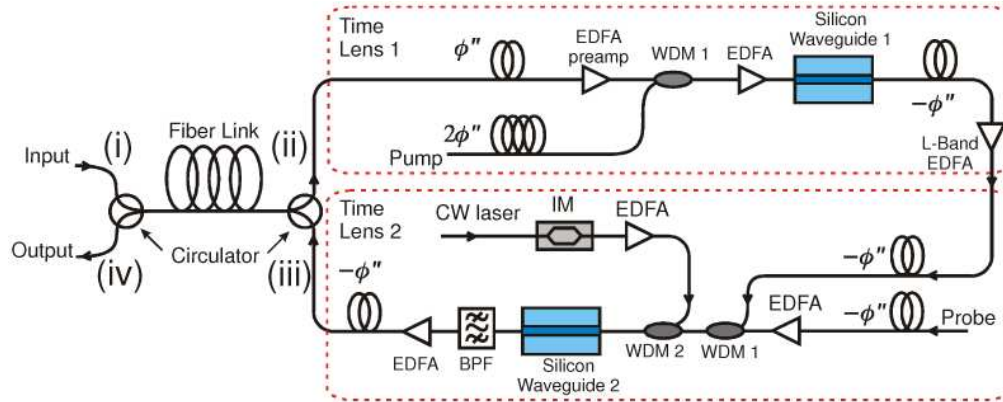


Fig. 3. (Color online) Schematic of the temporal imaging system. Two time-lens setups realize consecutive Fourier transformations on the signal with the output field being time-flipped and conjugated version of the input field in time. The amount of GDD applied to each path in the system is indicated on the figure, with $\phi'' \approx -22 \text{ ps}^2$. EDFA: Erbium-doped fiber amplifier, WDM: Wavelength division multiplexer, BPF: Band-pass filter, IM: Intensity modulator.

3. Experimental setup

The experimental setup to realize our SPC scheme in the presence of dispersive and nonlinear effects in fibers is sketched in Fig. 3. We test the compensation performance of our setup for individual pulse distortions introduced by GVD, TOD, and SPM in different fiber links. For the GVD case, we use a 300-m long SMF-28 fiber spool ($\phi_{GVD}'' = -6.5 \text{ ps}^2$), whereas for the TOD case, a combination of fibers [20-km SMF-28 and 4-km dispersion compensating fiber (DCF)] is utilized, which resulted in negligible GVD and an averaged dispersion slope of $\sim 0.11 \text{ ps}^3/\text{km}$ at the signal wavelength. The SPM case was tested with a 1-km-long highly

nonlinear fiber (HNLf) with negligible dispersion at the signal wavelength. The attenuation and nonlinear coefficients of HNLf are 0.9 dB and $10 \text{ (W} \cdot \text{km)}^{-1}$, respectively. The insertion loss of the HNLf is measured to be 2.9 dB and is due to the splicing loss between HNLf and SMF-28 patch cords. In order to perform SPC at the midpoint of a fiber link, we double-pass the signal pulses through the same fiber using a circulator pair.

The signal pulses are obtained from a modelocked fiber laser (38-MHz repetition rate, < 100 -fs pulses) by using a 4.5-nm wavelength-division multiplexing (WDM) filter centered at 1545 nm. Upon the first pass through the dispersive fiber link, the signal is sent into the SPC setup. The first FWM-based time lens is realized in a 15-mm-long silicon waveguide with a cross-sectional width and height of 550 nm and 300 nm, respectively. The pump for the first FWM is filtered from the same modelocked fiber laser output for synchronous operation with a 9-nm WDM filter centered at 1559 nm. The focal length of the first time lens is equivalent to the GDD introduced by 1-km SMF-28 fiber ($\phi_{p1}'' / 2 = \phi_{s1}'' \approx -22 \text{ ps}^2$). Pump and signal pulses are then synchronized in time and combined in a separate WDM filter. Both pulses are amplified with an EDFA and coupled into the first FWM silicon waveguide using a lensed fiber. The peak power level for the chirped pump coupled into the waveguide is estimated as 15.5 mW. The polarization states of both inputs were adjusted with fiber polarization controllers to match the transverse magnetic (TM) mode supported by the silicon waveguide. The first Fourier analyzer is completed by sending the generated idler at ~ 1572 nm through 200-m DCF such that $\phi_{i2}'' = -\phi_{i1}''$. A sample output spectrum after the first FWM stage is shown in Fig. 4(a), where the signal is temporally broadened prior to the SPC setup by the TOD-inducing fiber link. The time-to-frequency conversion of the signal pulse with TOD distortion is evident in the idler spectrum which is plotted in the inset of Fig. 4(a).

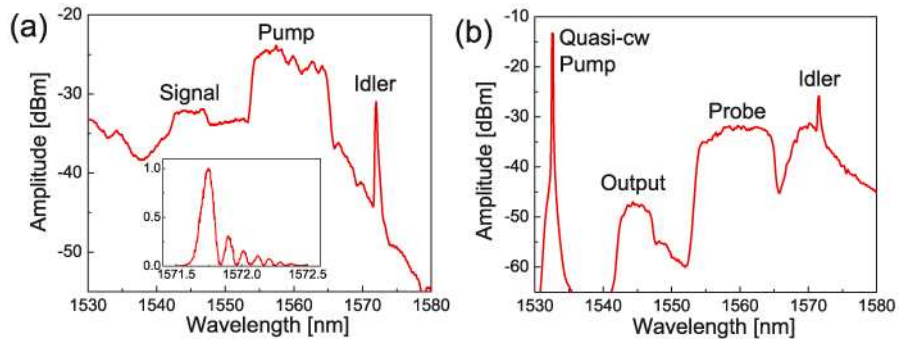


Fig. 4. (Color online) The output spectra recorded after (a) the first FWM stage and (b) the second FWM stage. The signal pulses are sent through the TOD fiber link with a dispersion slope of $\sim 0.11 \text{ ps}^3/\text{km}$. The inset in (a) shows the high-resolution trace of the idler spectrum after the first FWM stage, confirming time-to-frequency conversion.

The idler output of the first FWM stage is then filtered and amplified by an L-band EDFA for the second Fourier analyzer. The amplified idler output is used as a pump in the second FWM process to prevent consecutive conjugation of the temporal phase. The other FWM pump is derived from an intensity modulated tunable cw laser output to yield quasi-cw operation with high peak power. The tunable output is centered at 1532.7 nm to provide wavelength preserving SPC operation such that the idler output of the second FWM process is generated at the original input signal wavelength. For synchronous operation, the modulating RF signal is obtained from a fast photodiode which detects the modelocked fiber laser output. The output of the intensity modulator yields 250-ps pulses. The quasi-cw source is amplified and synchronized with the idler output from the first FWM stage. The probe input to the second time lens is tapped from the unchirped pump from the first time lens. In order to satisfy $\phi_{f2}'' / \phi_{f1}'' = -1$ condition, the dispersion imparted on the probe, ϕ_{p2}'' , matches the first

time-lens focal length with opposite sign, $\phi_{f2}'' = \phi_{p2}'' = -\phi_{f1}''$. Note that the wavelength separation between the amplified output from the first FWM stage and the probe input generates another FWM idler output at the original signal wavelength such that $E_{idler,2}(\tau) \propto E_{p2}^2(\tau)E_{idler,1}^*(\tau)$. In order to prevent interference between two FWM processes, the probe power level is kept lower than the amplified output from the first FWM stage and the quasi-cw source.

The polarizations of the input modes are aligned for the TM mode of the second silicon waveguide with a 15-mm length and a 700-nm \times 300-nm cross section. Input modes are combined with WDM filters and coupled into the second silicon waveguide with a lensed fiber. The output spectrum of the second FWM operation under the same operating conditions with the first time lens is plotted in Fig. 4(b). The FWM output generated at 1545 nm is filtered with a 9-nm bandpass filter, amplified with an EDFA, and passed through the last time-lens dispersive fiber before being coupled back into the circulator for the second pass through the fiber link.

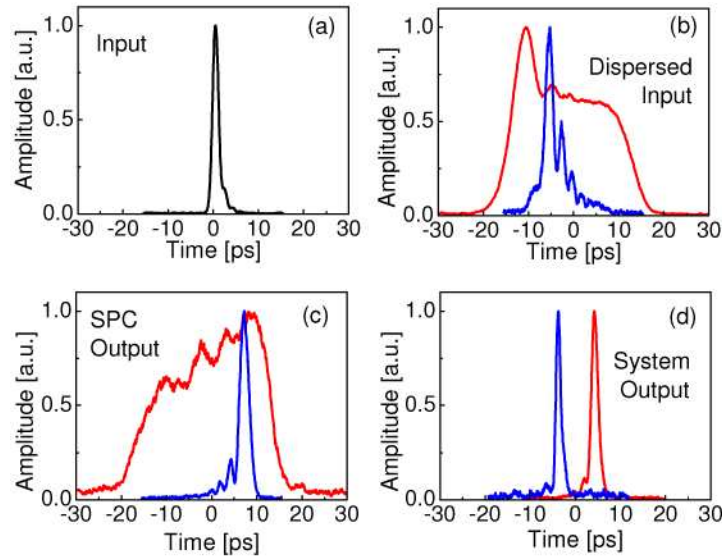


Fig. 5. (Color online) Cross-correlation of the signal pulses with GVD (red) and TOD (blue) compensation (a) before the circulator, (b) after the dispersive fiber, (c) after SPC, and (d) after final propagation through the dispersive fiber link. The pulses are intentionally separated for clarity. 1.5-ps input pulses are broadened to 30 and 20 ps for GVD- and TOD-inducing fiber links, respectively. The time-reversed and conjugated pulses after the SPC setup compress back to their original 1.5-ps duration.

4. Results

We first verify the chromatic dispersion compensation by measuring the optical cross-correlation of the signal at various stages of the experimental setup. For this purpose, an unfiltered output of the modelocked fiber laser is synchronized with the signal waveform for cross-correlation measurements at four locations (a-d) indicated in Fig. 5, which correspond to before and after the first and the second passes through the dispersive fiber link. As plotted in Fig. 5(b), the GVD (red) and TOD (blue) fibers cause significant broadening of the original signal pulse of ~ 1.5 -ps duration. In the case of GVD, the pulses are broadened to ~ 30 ps, whereas the TOD effect results in an asymmetric waveform of ~ 20 ps in temporal extent. The SPC operation of the temporal imaging system causes the time reversal of both dispersed waveforms, as plotted in Fig. 5(c). Upon the second pass through the dispersive fiber, both the GVD and TOD distorted pulses compress back to their original 1.5-ps duration. Thus, cross-correlation measurements verify that the temporal imaging SPC scheme compensates for both

odd and even orders of dispersion in optical fibers. We note that the maximum GVD and TOD broadening that can be compensated by our system is determined by the time-lens aperture. Any waveform that is temporally broadened beyond the time-lens pump or probe duration will be inherently clipped in the FWM process. Thus, the temporal extents of the dispersed pump and probe define the limits on tolerable signal dispersion. In our case the second time-lens probe, which is sent through a smaller amount of dispersion, sets the temporal aperture of the imaging system ($\Delta T = \beta_{p2}^{(2)} L_{p2} \Delta f_{p2} \sim 150$ ps). Therefore, if the combination of the dispersive fiber link and the time-lens input and output fibers incurs pulse broadening beyond ΔT , the waveform will be clipped in the second FWM process. This temporal aperture may be extended by increasing the bandwidths of the time-lens pump and probe until TOD effects in the time-lens fibers become significant [36].

We then characterize our system for compensation of nonlinear distortions introduced by SPM. In order to induce SPM on signal pulses, we replace the fiber link in Fig. 3 with a 1-km-long HNLF and move the first time-lens pre-amplifier EDFA in the signal arm before the HNLF to provide sufficient peak power. The signal bandwidth is reduced to 1-nm by inserting an additional tunable filter to accommodate for the spectral broadening in HNLF, and the center wavelength is shifted to 1542.5 nm. When the average power level of the signal before being coupled into HNLF reaches 0.1 mW, significant distortion in the signal spectrum is observed due to SPM [Fig. 6(a)]. At this power level, we estimate the accumulated nonlinear phase shift as π radians. The conjugated signal output after the SPC system is amplified and coupled back into the HNLF. The output signal spectrum is recorded as a function of the amplification level in the final EDFA of the temporal imaging system, as shown in Fig. 6(b). When the conjugated signal power is low, the SPM is uncompensated and the signal spectrum is distorted. As the EDFA gain is increased, the conjugated signal spectrum starts to compress, eventually reaching the original signal bandwidth after the tunable filter. We attain the narrowest output bandwidth when the average power of the conjugated signal is approximately 0.1 mW. Beyond this power level, the output spectrum broadens again due to the uncompensated nonlinear phase shift.

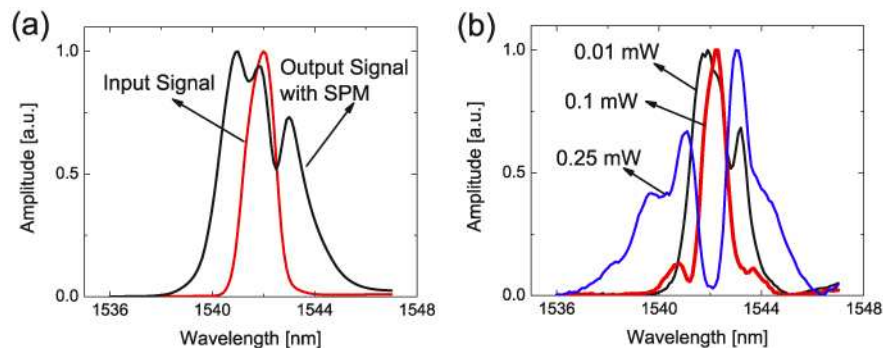


Fig. 6. (Color online) (a) Spectra of signal pulses before and after the HNLF. The nonlinear phase shift is estimated to be π radians for 0.1 mW average signal power coupled into the HNLF. (b) Conjugated signal spectra upon the second pass through the HNLF. Compensation of spectral broadening is shown for various back-coupled conjugated signal power levels. Under-compensated (0.01 mW), compensated (0.1 mW), and over-compensated (0.25 mW) spectra are indicated.

We note that the maximum nonlinear phase shift that can be compensated in our system depends on the initial chirp, the bandwidth of the signal, and the temporal aperture of the time lens. The SPM-induced nonlinear phase shift causes additional temporal broadening or compression of the signal envelope upon passing through the dispersive fibers in the time-lens setup [44]. The duration of the signal envelope can exceed the probe temporal window if the nonlinear phase shift is excessive. Following the analytical treatment in Ref [44], we calculate the maximum permissible nonlinear phase shift for which the temporally-broadened signal

duration ($1/e^2$ -width) is equivalent to the time-lens temporal window, which is determined by the chirped probe width of 150 ps. For the existing system parameters, the maximum nonlinear phase shift that can be compensated is calculated as 1.8π radians, given that the main contribution to GVD comes from time-lens fibers and signal bandwidth is 1 nm. Similar to the chromatic dispersion case, larger nonlinear phase shifts can be compensated if time-lens pump and probe bandwidths are increased. We note that full SPM compensation with SPC can be obtained only when the loss in the nonlinear medium is very low or negligible [4]. Since nonlinear pulse evolution in the optical fiber is strongly coupled to the pulse amplitude, additional caution must be taken to control SPM-induced spectral broadening in the presence of loss. SPC induces a time-reversed evolution of the pulse for the second pass through the nonlinear medium, thus any loss mechanism that is incurred in the first pass must be accompanied by a gain mechanism in the second pass. This approach has already been shown to be effective for TPC demonstrations where the loss in the first half of the fiber link is compensated by the gain provided by reverse Raman pumping in the second half [45,46].

5. Conclusion

In summary, we demonstrate a temporal imaging system based on broadband FWM in silicon waveguides to implement midpoint spectral phase conjugation for dispersion and nonlinearity compensation in optical fibers. By engineering the Fourier imaging properties of FWM-based time lenses, we provide the necessary time reversal and conjugation of the input fields to compensate for GVD, TOD, and SPM in various different types of fibers. The pump, probe, and quasi-cw inputs to two-stage FWM configuration in silicon waveguides can be controlled to prevent the center frequency shift of the conjugated output. A practical limitation on tolerable input dispersion and nonlinearity using this technique comes from the finite time-lens aperture, which can be enhanced by increasing the pump and probe bandwidth. While SPC operation is demonstrated to compensate for individual impairments, the combination of these effects should also be compensated with our configuration as long as the distorted signal pulse does not exceed the temporal window of the time lenses. Furthermore, as long as the input power levels are within the dynamic range of the EDFA's and uncompensated nonlinearities from FWM operations are avoided, the performance of our scheme is robust against fluctuations in the input power levels once the ideal system gain is achieved for the optimal dispersion and SPM compensation. Our temporal imaging scheme offers a compact and easily configurable alternative for dispersion compensation and data recovery in long-haul optical fiber communication systems.

Acknowledgements

We acknowledge financial support from the DARPA DSO OAWG Program and the Center for Nanoscale Systems, supported by the NSF and the New York State Office of Science, Technology & Academic Research. This work was performed in part at the Cornell NanoScale Science & Technology Facility, a member of the National Nanotechnology Infrastructure Network, which is supported by the National Science Foundation (Grant ECS-0335765).